

Cite this: *Dalton Trans.*, 2019, **48**, 7693Received 25th February 2019,
Accepted 26th April 2019

DOI: 10.1039/c9dt00841a

rsc.li/dalton

Regression analysis of properties of [Au(IPr)(CHR₂)] complexes†Richard M. P. Veenboer,^a Luis Miguel Azofra,^{b,c} Danila Gasperini,^d Alba Collado,^e David B. Cordes,^a Alexandra M. Z. Slawin,^a Luigi Cavallo^f and Steven P. Nolan^{g,h}

New [Au(IPr)(CHR₂)] complexes have been synthesised through protonolysis reactions of [Au(IPr)(OH)] with moderately acidic substrates, CH₂R₂. An array of spectroscopic (IR and NMR), structural (X-ray), electronic (DFT) and experimental (reactivity) parameters was collected to quantify the variation in stereoelectronic properties of these new and previously reported [Au(IPr)(CHR₂)] complexes. Variation of the R substituents on the carbanion ligands (CHR₂[−]) was found to have a crucial impact on parameters characterising the resulting gold complexes. A regression analysis of both experimental and modelled parameters, guided by network analysis techniques, produced linear models that supported trends within the [Au(IPr)(CHR₂)] complexes.

Introduction

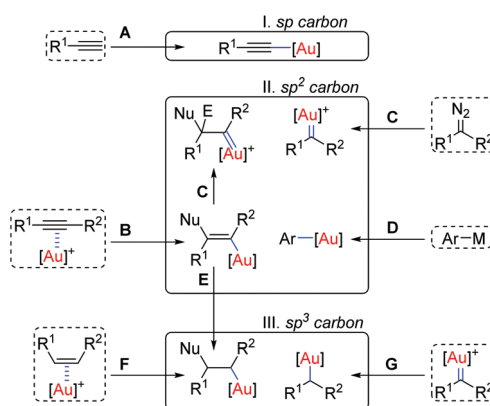
The use of homogeneous gold chemistry has uncovered and helped develop a plethora of useful catalytic organic transformations.¹ Next to many gold-catalysed procedures that rely on π -activation of unsaturated substrates,² development of applications in the functionalization of C–H bonds has gained increased attention.³ Study of gold-bound intermediates in these organic transformations provides important information

about the role of ligands in defining the optimum gold system to use.⁴ A combination of relativistic effects alters the size of the atomic orbitals on gold⁵ and gives rise to complexes with stronger bonds to gold than its group congeners.⁶ All different hybridisation states of carbon are encountered in gold-bound species (Scheme 1).

Those containing gold bound to sp-hybridised carbon atoms are readily formed from alkynes (Scheme 1, reaction A)⁷ and a variety of vinyl-gold, aryl-gold and carbenoid species with sp²-hybridised carbons have been proposed as intermediates in numerous processes (Scheme 1, reactions B–D).⁸

^aEaStCHEM, School of Chemistry, University of St Andrews, North Haugh, St Andrews, KY16 9ST, UK^bCIDIA-FEAM (Unidad Asociada al Consejo Superior de Investigaciones Científicas, CSIC, avalada por el Instituto de Ciencia de Materiales de Sevilla, Universidad de Sevilla), Instituto de Estudios Ambientales y Recursos Naturales (i-UNAT), Universidad de Las Palmas de Gran Canaria (ULPGC), Campus de Tafira, 35017 Las Palmas de Gran Canaria, Spain^cDepartamento de Química, Universidad de Las Palmas de Gran Canaria (ULPGC), Campus de Tafira, 35017 Las Palmas de Gran Canaria, Spain^dDepartment of Chemistry, University of Bath, Claverton Down, Bath, BA2 7AY, UK^eDepartamento de Química Orgánica and Centro de Innovación en Química Avanzada (ORFEO-CINQA), Facultad de Ciencias Químicas, Universidad Complutense, 28040 Madrid, Spain^fKAUST Catalysis Center (KCC), King Abdullah University of Science and Technology (KAUST), Thuwal 23955-6900, Saudi Arabia^gDepartment Chemistry and Center for Sustainable Chemistry, Ghent University, Krijgslaan 281, S-3, 9000 Ghent, Belgium. E-mail: steven.nolan@ugent.be^hDepartment of Chemistry, College of Science, King Saud University, P. O. Box 2455, Riyadh 11451, Saudi Arabia

† Electronic supplementary information (ESI) available: Experimental details including copy of the spectra of all the compounds, crystallographic information, tables of all parameters investigated and details about the computational study and statistical analysis. CCDC 1811379–1811384. For ESI and crystallographic data in CIF or other electronic format see DOI: 10.1039/c9dt00841a



Scheme 1 Formation of carbon-bound gold species with different carbon hybridisations. sp: (A) σ -activation. sp²: (B) π -activation and nucleophilic addition; (C) carbene transfer; and (D) transmetalation. sp³: (E) hydrogen shift; (F) slippage; and (G) addition to carbenoid. [Au] = Au(L), with L = PR₃ or NHC.

Catalytic reactions that involve intermediates with sp^3 -hybridised carbons bound to gold are far less common.⁹ This reactivity trend correlates with the fundamentally less reactive nature of $C(sp^3)$ -H compared to $C(sp^2)$ -H and $C(sp)$ -H bonds and follows the pK_a values (in water) of methane (48), ethylene (44) and acetylene (25).¹⁰ Despite their rare occurrence in catalytic transformations, many $C(sp^3)$ -bound gold complexes have been prepared and their properties have been studied.¹¹ Selected formations of these complexes involve: (i) hydrogen shift reactions (Scheme 1, reaction E);^{9a} (ii) slippage of η^2 -alkene to η^1 -alkene complexes (Scheme 1, reaction F);¹² and (iii) nucleophilic addition to gold carbenoids (Scheme 1, reaction G).^{13,14}

The synthesis and exploration of NHC-gold(i) chloride, $[Au(IPr)Cl]$ (**1**),²² and NHC-gold(i) hydroxide, $[Au(IPr)(OH)]$ (**2**),²³ complexes in particular continue to open new venues in homogeneous gold chemistry.²⁴ These efforts have paved the way for the investigations of NHC-gold(i) complexes supported by ligands based on sp^3 -hybridised carbon centres, $[Au(IPr)(CHR_2)]$ (Fig. 1). A substitution reaction of **1** with a dimethyl zinc reagent formed $[Au(IPr)(CH_3)]$ (**3**),²⁵ and a simple protonolysis reaction of **2** with acetone formed NHC-gold(i) acetyl complex, $[Au(IPr)(CH_2C(O)CH_3)]$ (**4**) (Fig. 1).²⁶ Reaction of this latter complex with weak acids, such as acetylacetone and dimethyl malonate formed $[Au(IPr)(CH(C(O)CH_3)_2)]$ (**5**) and $[Au(IPr)(CH(C(O)OCH_3)_2)]$ (**6**), respectively (Fig. 1).²⁶ The ability of **2** to deprotonate acids up to pK_a 30.3 (in DMSO),²⁷ encouraged us to extend the range of known IPr-based complexes **3–6** to those of other organic substrates containing sufficiently acidic $C(sp^3)$ -H bonds (Fig. 1). The complex from acetophenone, $[Au(IPr)(CH_2C(O)Ph)]$ (**7**), was targeted to diversify the range of complexes containing ketone and ester moieties (Fig. 1). A precedent in phosphine-gold containing nitrile functional groups,²⁷ prompted us to examine reactions with acetonitrile,²⁸ malononitrile and phenylacetonitrile to form $[Au(IPr)(CH_2CN)]$ (**8**), $[Au(IPr)(CH(CN)_2)]$ (**9**) and $[Au(IPr)(CH(Ph)CN)]$ (**10**) (Fig. 1). To complement the range of

complexes derived from low molecular weight solvents (acetone and acetonitrile), the complexes derived from nitromethane and nitroethane, $[Au(IPr)(CH_2NO_2)]$ (**11**) and $[Au(IPr)(CH(CH_3)NO_2)]$ (**12**), were also targeted (Fig. 1). We aimed to gain an understanding of the influence of the various CHR_2^- ligands on the properties of the corresponding IPr-gold(i)-carbanion complexes by analysing a range of parameters associated with substrates CH_2R_2 and complexes $[Au(IPr)(CHR_2)]$ (**3–12**): pK_a values²⁹ of the CH_2R_2 starting materials (Fig. 1), the Hammett parameters, σ_m and σ_p ,³⁰ of their R groups, spectroscopic values (NMR chemical shifts and IR stretching frequencies) as well as parameters from solid-state structures and computationally modelled structures.

Considering NHC ligands and gold chemistry, some insightful linear models based on such data include those between redox potentials and orbital energies,³¹ between NMR chemical shifts of different nuclei³² and between different theoretical parameters.³³ Models have also been described that relate single parameters to linear combinations of multiple other ones such as orbital energies *versus* combinations of bond length and bond angle,³⁴ or atomic orbital components (%s-character) *versus* a combination of covalent radii and electronegativity values.³⁵

Relations between parameters can either be pursued deliberately, or researchers might spot them through careful analysis of their data. The generation of hypotheses is particularly non-trivial when many parameters are available or when point-to-plane relations are sought. This work chiefly aims to demonstrate the use of "hypothesis generating techniques"³⁶ for the analysis of the data associated with $[Au(IPr)(CHR_2)]$ (**3–12**). High-level qualitative hypotheses about the influence of the CHR_2^- ligands on the properties of **3–12** were first formed based on literature precedent and inspection of constants (pK_a values and Hammett parameters) and data obtained from routinely available experimental techniques (IR, NMR). Solid-state structures were next determined and both computational modelling studies and kinetic experiments were conducted to collect a wealth of additional data about these complexes. A pragmatic statistical analysis was then employed to turn the large number of possible relations between the different parameters into a tractable number of candidates to be used for the quantitative description of the initial hypotheses. This approach was expected to lead to statistically significant linear relations that might have been hard to find by chemical intuition alone.

Results and discussion

Synthesis of carbanion complexes

Complexes $[Au(IPr)(CHR_2)]$ (**7–12**) were formed as air and moisture stable solids through facile protonolysis reactions of $[Au(IPr)(OH)]$ (**2**) with stoichiometric or excess amounts of the corresponding substrate (Fig. 2).³⁷ Pure products could generally be isolated after a simple precipitation step. Clean conversions of **2** to $[Au(IPr)(CH_2COPh)]$ (**7**) was observed with only

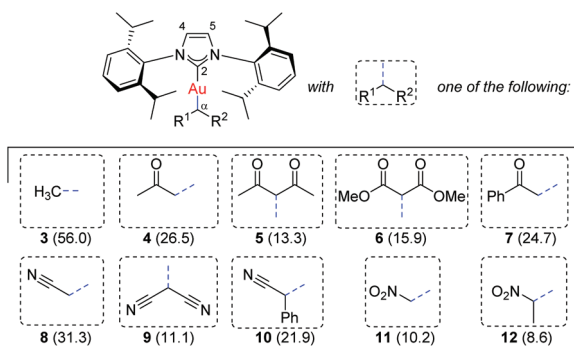


Fig. 1 Structure of $[Au(IPr)(CHR_2)]$ (**3–12**) and range of complexes with different carbanion ligands (CHR_2^-) used in this study.¹⁵ pK_a values (in DMSO) of substrates (CH_2R_2) are given in parentheses: methane,¹⁶ acetone,¹⁶ acetylacetone,¹⁷ dimethyl malonate,¹⁸ acetophenone,¹⁹ acetonitrile,¹⁹ malononitrile,¹⁹ phenylacetonitrile,¹⁹ nitromethane,²⁰ and nitroethane.²¹

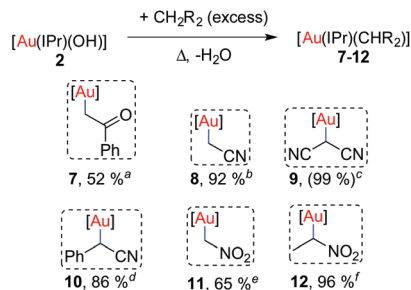


Fig. 2 Synthesis of $[\text{Au}(\text{IPr})(\text{CHR}_2)]$ (7–12) from **2**. Isolated yields are given, $[\text{Au}] = \text{Au}(\text{IPr})$. ^a 1.1 equiv. acetophenone, 20 hours in benzene-*d*₆ at 60 °C. ^b 20 hours in acetonitrile at 80 °C. ^c 10 equiv. malononitrile, 1 hour in toluene at 60 °C, conversion to **9** was measured using mesitylene as internal standard. ^d 1 equiv. phenylacetonitrile, 1 hour in toluene at 80 °C. ^e 1 hour at 60 °C in nitromethane. ^f 2 hours at 60 °C in nitroethane.

1.1 equivalents of acetophenone. Unidentified side-products formed in stoichiometric reactions of malononitrile and nitroethane with **2** in chloroform at 60 °C.³⁸ Use of an excess of substrate in toluene, however, permitted formation of $[\text{Au}(\text{IPr})(\text{CH}(\text{CN})_2)]$ (**9**) and $[\text{Au}(\text{IPr})(\text{CH}(\text{CH}_3)\text{NO}_2)]$ (**12**), selectively. Isolation of **9** from an excess of malononitrile, however, proved difficult and only minor amounts of pure material could be obtained from an un-optimized purification procedure that involved multiple recrystallization steps. $[\text{Au}(\text{IPr})(\text{CH}_2\text{CN})]$ (**8**), $[\text{Au}(\text{IPr})(\text{CH}(\text{Ph})\text{CN})]$ (**10**) and $[\text{Au}(\text{IPr})(\text{CH}_2\text{NO}_2)]$ (**11**) were formed by heating **2** in acetonitrile, phenylacetonitrile or nitromethane, respectively.

Spectroscopic study

Complexes $[\text{Au}(\text{IPr})(\text{CHR}_2)]$ (**3**–**12**) were characterised by solution-phase ¹H and ¹³C{¹H} NMR spectroscopy (in CDCl₃) and by ATR-FTIR spectroscopy (solid state). Trends in differences of chemical shift values and stretching frequencies, compared to those of literature values corresponding to constituting substrates CH₂R₂, supported the expected transfer of electron density from the negatively charged carbanion (CHR₂[−]) to the positively charged $[\text{Au}(\text{IPr})]^+$ fragment (Table 1).³⁹

Table 1 Observations in $[\text{Au}(\text{IPr})(\text{CHR}_2)]$ (**3**–**12**) (part A)^a

Entry	Substrate	Complex	Phenomenon
1			Redshifted IR stretching frequencies: $55 \pm 18 \text{ cm}^{-1}$. ^b
2			Shielded ¹ H chemical shift: 0.01–1.21 ppm. ^c

^a All values are listed in the ESI. ^b Observed in complexes **4** and **6**–**12**. ^c Observed in complexes **3**, **4** and **6**–**12**.

Statistically significant redshifts of $55 \pm 18 \text{ cm}^{-1}$ (*t*-test, *p*-value < 0.01)⁴⁰ were found in the stretching bands of the infrared-active functional groups on the carbanion ligands (CHR₂[−]) of complexes $[\text{Au}(\text{IPr})(\text{CHR}_2)]$ (**4** and **6**–**12**) relative to those in the unbound substrates (CH₂R₂) (Table 1, entry 1). Likewise, all experimental chemical shifts of complexes **3**, **4** and **6**–**12** C^αH-δ(¹H) in $[\text{Au}(\text{IPr})(\text{CHR}_2)]$ were 0.01–1.21 ppm lower (*t*-test, *p*-value = 0.02) than C^α-δ(¹H) values in the corresponding CH₂R₂ (Table 1, entry 2). The complex derived from acetylacetonone, $[\text{Au}(\text{IPr})(\text{CH}(\text{COCH}_3)_2)]$ (**5**), was found to break this trend, with a 14 cm^{−1} blue-shifted IR stretching frequency, $\tilde{\nu}_{\text{C}=\text{O}}$, and 0.29 ppm deshielded C^α-δ(¹H) chemical shift. This was expected, since coordination to gold would disrupt electron delocalisation in the acetylacetonate moiety and thus increase the effective electron density in the carbonyl functional groups.

Measurement of relative rates of protodeauration

The relative reactivities of a series of PPh₃-gold(i) complexes containing Au–C with different carbon hybridisations have previously been measured experimentally.⁴¹ Following a similar approach, the relative reactivities of $[\text{Au}(\text{IPr})(\text{CHR}_2)]$ (**3**–**12**), *k*_{rel}, were quantified by measuring their relative susceptibilities to protodeauration by means of competition experiments in the presence of limiting amounts of hydrogen chloride (Fig. 3).⁴²

A scale was thus obtained with the fastest protodeauration rate measured for $[\text{Au}(\text{IPr})(\text{CH}(\text{CH}_3)\text{NO}_2)]$ (**12**), and the slowest one for $[\text{Au}(\text{IPr})(\text{CH}_2\text{CN})]$ (**8**). Values of *k*_{rel} as well as logarithm-transformed values, log *k*_{rel},⁴³ were added to dataset for complexes **3**–**12**. Qualitatively, complexes bearing carbanion ligands with ketone groups (**4**, **5** and **7**) displayed higher tendencies to protodeauration compared to those with nitrile groups (**8**–**10**), but not compared to those bearing nitro substituents (**11**–**12**). Within the series of complexes $[\text{Au}(\text{IPr})(\text{CH}_2\text{COCH}_3)]$ (**4**), $[\text{Au}(\text{IPr})(\text{CH}(\text{COCH}_3)_2)]$ (**5**) and $[\text{Au}(\text{IPr})(\text{CH}_2\text{C}$

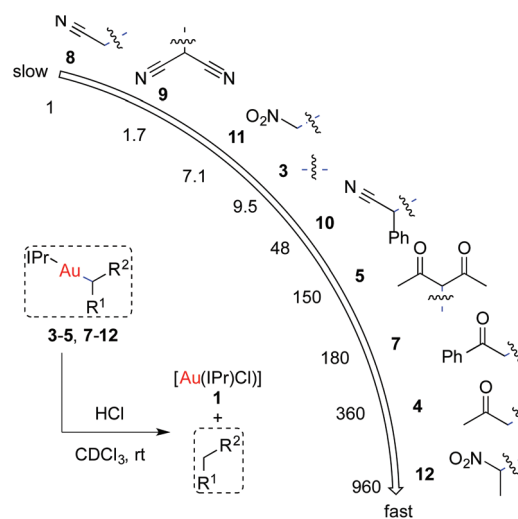


Fig. 3 Relative rates, *k*_{rel}, of protodeauration of $[\text{Au}(\text{IPr})(\text{CHR}_2)]$ (**3**–**5** and **7**–**12**).

(O)Ph]] (7), relative protodeauration rates were found to be approximately inversely proportional to the pK_a value of the CH_2R_2 substrates (Fig. 2).

No clear trend was found between the relative protodeauration rates of complexes containing methyl (3) or nitro (11–12) functional groups. Higher degrees of substitution in complexes bearing nitro groups (12 *versus* 11) and nitrile groups (9 and 10 *versus* 8) appeared to lead to faster rates of protodeauration as might be associated with the relative steric compressions.⁴⁴ The relatively fast protodeauration of $[Au(IPr)(CH(Ph)CN)]$ (10) as compared to that of 8 and 9 was considered a consequence of additional stabilisation of a charged intermediate imposed by the neighbouring aromatic ring.⁴⁵

X-Ray structure determination

Crystals suitable for X-ray diffraction analysis were grown of complexes 7–12 (Fig. 4). In these complexes, Au–C² and Au–C^α (C² and C^α refer to the carbene and carbanion carbons, respectively, Fig. 1) bond lengths of 2.00–2.02 Å and 2.06–2.11 Å, respectively, were as expected for IPr–gold(i) complexes and similar to previous examples.²⁶ The solid-state geometries of all complexes $[Au(IPr)(CHR_2)]$ (3–12), both previously reported structures of 3–6 and the new 7–12 were used to compute theoretical models (DFT).⁴² The subsequent analyses have been conducted with coordinates and derived para-

eters of both experimental and modelled structures. Closer inspection of bond lengths and angles of revealed four clear trends (Table 2) and it was postulated that the geometry of $[Au(IPr)(CHR_2)]$ (3–12) presented an optimal arrangement for the transfer of electron density the strongly donating carbanion ligands (CHR_2^-) to the positively charged $[Au(IPr)]^+$ fragment:

(i) *Elongation of Au–C² bonds*: Significantly longer Au–C² bond lengths (by 0.053–0.096 Å for experimental and by 0.084–0.134 Å for modelled structures) in 3–12 compared to $[Au(IPr)Cl]$ (1) (1.942 Å; *t*-test, *p*-values <0.01)²² indicated that the carbanion ligands CHR_2^- exerted a larger *trans* influence compared to chloride (Table 2, entry 1).⁴⁶

(ii) *Bending of C²–Au–C^α bond*: $\angle C^2-Au-C^\alpha$ angle appeared to be bent away from a linear conformation in complexes 4–12 (Table 2, entry 2). Average values of $176.9 \pm 1.9^\circ$ (experimental) and $176.1 \pm 1.9^\circ$ (modelled) were significantly lower than 180° (*t*-test, *p*-values: both <0.01). Bending of similar magnitude has previously been observed in a series of $[Au(I^tBu)X]$ (X includes ONO_2 , Cl and CH_3).⁴⁶ Deviation of linearity of gold(i) complexes has previously been shown to lead to maximisation of orbital overlap for enhanced π -backbonding and stabilisation.⁴⁷ This bending was considered an indication that π -backbonding would occur from gold both to the IPr: and the CHR_2^- ligands, a hypothesis that was later looked at through computational modelling studies.

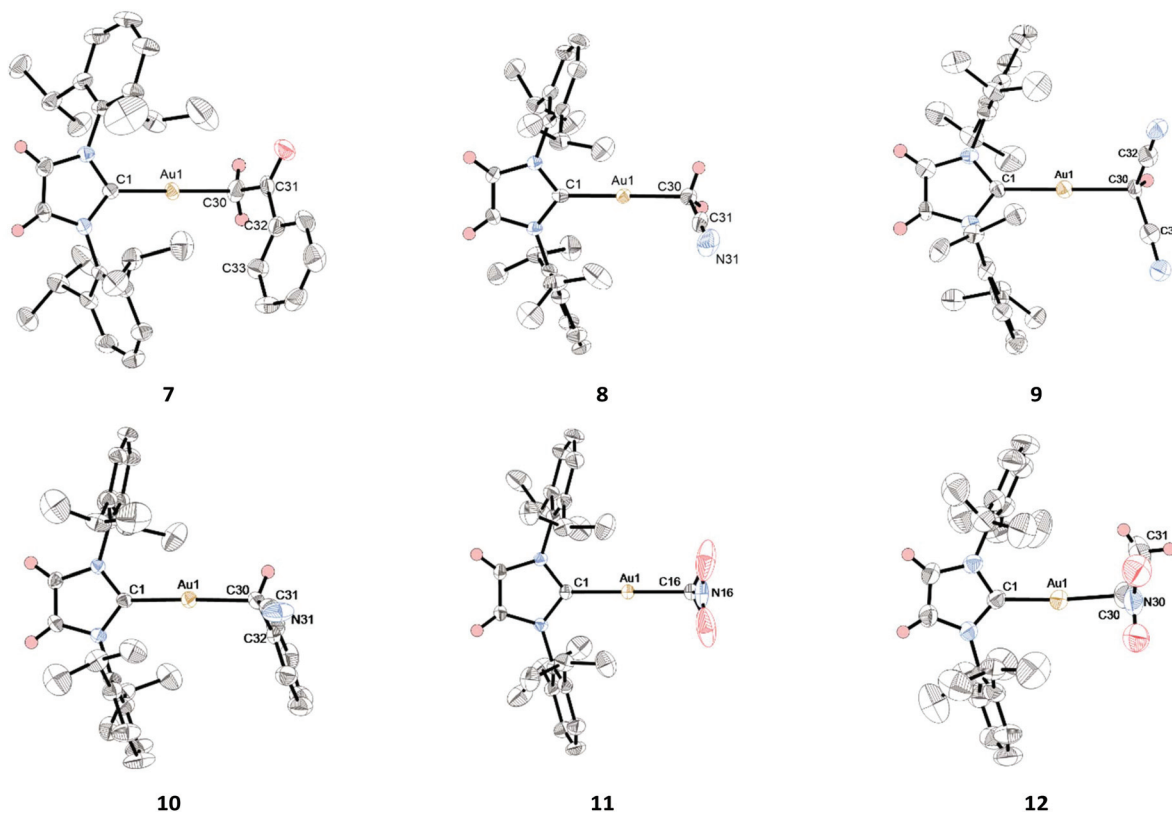


Fig. 4 Thermal ellipsoid representations of $[Au(IPr)(CHR_2)]$ (7–8 and 10–12) at 50% probability. Most hydrogen atoms and molecules of solvent are omitted for clarity. Representations in orientations that more clearly show the geometries of the carbanion ligands (CHR_2^-) and assignments of atom numbers to labels C² (*i.e.*, C1) and C^α (*i.e.*, C16 or C30) are given in the ESI.†

Table 2 Observations in [Au(IPr)(CHR₂)] (3–12) (part B)^a

Entry	Expected	Observed	Phenomenon ^b
1			Au–C ² elongation: ^c 2.016 ± 0.013 Å
2			Bending: ^d ∠C ² –Au–C ^α = 176.9 ± 1.9°
3			Flattening of CHR ₂ [−] : ^e θ = 18.4 ± 1.5°
4			Twist of NHC: ^c ∠N ¹ –C ⁵ –C ⁴ –N ³ = 0.35 ± 0.29°

^a All values are listed in the ESI. ^b Values are derived from experimental structures. ^c Observed in complexes 3–12. ^d Observed in complexes 4 and 6–12. ^e Droop angle,⁴⁹ observed in complexes 3–12.

(iii) *Flattening of CHR₂[−] and rehybridisation in C^α*: A comparison of structural parameters of complexes 4–12 to literature values of analogues bearing tertiary phosphine ligands indicated that the carbanion ligands (CHR₂[−]) flattened more in [Au(IPr)(CHR₂)] than in the corresponding [Au(PR₃)(CHR₂)] complexes (Table 2, entry 2).⁴⁸ This phenomenon could be quantified by the Droop angle for C^α, θ,⁴⁹ that measures the deviation from a perfectly tetrahedral arrangement of substituents.⁵⁰ Average Droop angles for the carbanion ligands (CHR₂[−]) in 3–12 of 18.4 ± 1.5° and 16.7 ± 3.1° were measured in the experimental and modelled structures, respectively. Only the latter values were significantly lower than 19.5° (*t*-test, *p*-values: 0.07 and 0.02). The relation between hybridisation and electron distribution amongst *s* and *p* orbitals follows from Coulson's Orthogonality Theorem,⁵¹ and the %*s*-character parameter in the C^α–Au bond (Coulson's σ parameter), σ(C^α–Au), was calculated from the structural data.⁵² Average values for 3–12 of 22 ± 4% (experimental) and 19 ± 7% (modelled) were found to be different and in most cases lower than 25%⁵³ *s*-character. As with the Droop angle, this trend could only be supported for the modelled, but not for the experimental values, with *p*-values from the *t*-test of 0.02 and 0.06, respectively.

(iv) *Ring twist of NHC*: Deviation of angle ∠N¹–C⁵–C⁴–N³ from 0° was indicative of a ring twist of the NHC (Table 2, entry 3). The average value of ∠N¹–C⁵–C⁴–N³ in 3–12 of 0.35 ± 0.29° in the experimental structures and to 0.13 ± 0.10° in the modelled ones were modest compared to those previously measured for [Au(IPr)Cl] (1, 1.30°)²² and for [Au(IPr)(OH)] (2, 0.62°).²³ This ring twist has previously been described to influence the proximity of the *N*-substituents of the NHC to the gold centre.⁵⁴ Variations in values of this parameter within the series 3–12 were considered as a probe for other electronic effects as well.

Computational modelling of electronic properties

To validate the spectroscopic (Table 1) and structural trends (Table 2) observed in [Au(IPr)(CHR₂)] (3–12), electronic properties were studied by means of computational modelling. Description of bonding between metal centres and ligands by Dewar, Chatt and Duncanson in terms of bonding and back-bonding interactions (DCD model)⁵⁵ has proved a powerful approach and provided a better understanding of the electronic structure of species relevant to gold catalysis.⁵⁶ The π-accepting properties of NHCs next to their σ-donor properties dictate that bonding and back-bonding interactions should be decomposed in components of different symmetries.⁵⁷ In that context, a computational energy decomposition analysis (EDA) was performed for the C²–Au and C^α–Au bonds in selected complexes [Au(IPr)(CHR₂)] (3, 5, 6, 9 and 11) and a range of energy parameters were obtained: C^x–E_y^{L→M}, with *x* = 2, α to indicate values associated with C² or C^α, *y* = σ, π to indicate the symmetry of the interaction and *z* = →, ← or ↔ to indicate the direction of the interaction (bonding, back-bonding or total).

The relative values of E_σ^{L→M} and E_π^{L→M} were indicative of stronger σ-bonding interactions in the Au–C^α bonds than in Au–C² bonds, but the strength of the π-bonding interactions remained similar in those bonds (Table 3). These interactions were furthermore expressed in values for relative donation and backdonation of σ-symmetry and π-symmetry in the two bonds, %E_σ and %E_π (Table 3). The similarly proportioned σ-bonding components from C^α and C² to gold exceeded σ-back-bonding contributions from gold. The π-symmetric bonding component in Au–C^α consisted of a slightly stronger donating component, whereas the π-symmetric bonding component in Au–C² was strongly back-donating (gold to C²) in nature. These values indicated: (i) that the Au–C^α bond was slightly stronger than the Au–C² one (unlike the relative bond lengths suggested, Table 2, entry 1); and (ii) that a bonding interaction with π-symmetry resulted in a net electron density from the carbanion ligand (CHR₂[−]) to the NHC ligand, as expected in an arrangement with occupied and empty *p* orbitals on those respective ligands.

Other parameters were computed and included in the dataset for [Au(IPr)(CHR₂)] (3–12):⁵⁸ C_s^α ≥ 0.5, the (constrained) %*s*-component of the hybrid orbital on C^α occupied by the lone pair on fragments CHR₂. Wiberg bond orders for the bonds Au–C², Au–C^α and C^α–H^α (indicated with symbol B)⁵⁹ and Mulliken populations of the Au, C² and C^α atoms (indicated with symbol M).⁶⁰

Finding relations between parameters

Data from different sets of parameters (component, EDA, Hammett, IR, NMR, Order, pK_a, population, rate and structure)

Table 3 Average EDA parameters E_σ and E_π (in absolute values and percentage)

	Au–C ^α	Au–C ²		Au–C ^α	Au–C ²
E _σ ^{L→M}	−72 ± 6	−56 ± 4	%E _σ	58 ± 5	54 ± 1
E _π ^{L→M}	−10 ± 2	−11 ± 0	%E _π	61 ± 7	15 ± 0

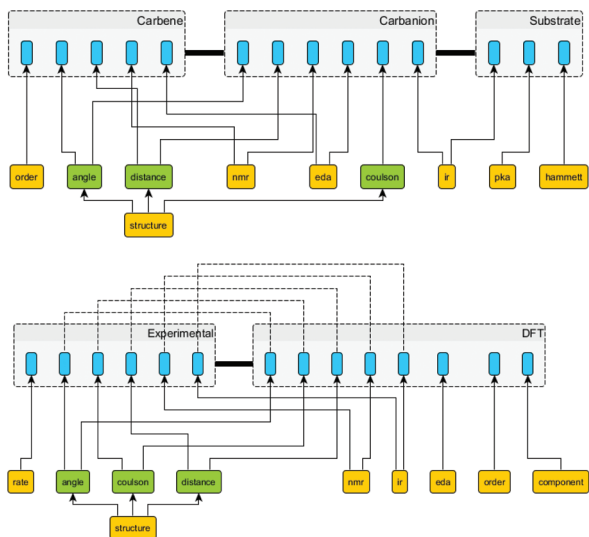


Fig. 5 Grouping of parameters from different sets. Colour code: Yellow = set, green = subset, blue = variables. Top refers to parameters associated with different parts of complexes, while bottom refers to parameters derived from different methods.

were grouped according to the moieties of the complexes that they were associated with (*i.e.*, carbene, carbanion of original substrate, Fig. 5a) or the method that was used to acquire the data (*i.e.*, experimental or DFT, Fig. 5b).

Potential relations between parameters included:

(i) Properties of sites (*i.e.*, atoms or bonds) in substrates *versus* those in complexes.

(ii) Properties of sites (*i.e.*, atoms or bonds) in the different ligands of complexes (*i.e.*, carbene and carbanion);

(iii) Experimental data *versus* the analogous data obtained from computational modelling (DFT).

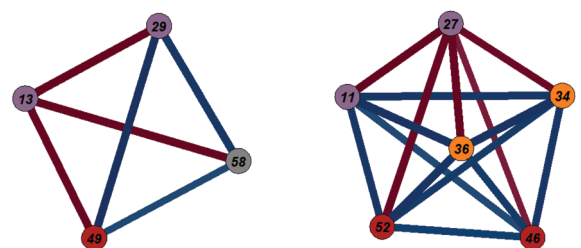
(iv) Manifestations (*e.g.*, relative protodeauration rates) *versus* structural, spectroscopic (*i.e.*, NMR and IR) or electronic (*i.e.*, component, EDA) properties. Note that no parameters related to the nature of the carbanion ligand (*i.e.*, degree of substitution, type of substituents or possibility of electron delocalisation) are included in this analysis.

Statistical analysis of all data collected for [Au(IPr)(CHR₂)] (3–12) resulted in groups of parameters from different sets that were used as starting point for further analysis.⁶⁴ Possible relations between different parameters within each group were visualised by representing these as edges in a graph with vertex weights defined by the correlation of pairs of parameters (Fig. 6):

1. Positive correlations were found between C²-E_π^{L←M} (EDA), C²-δ(¹³C) (NMR, modelled)⁶⁵ and pK_a, whereas negative correlations were found between these three parameters and C^α-E_π^{L→M} (EDA) (Fig. 6a, group 1).

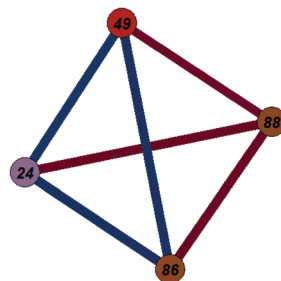
2. A subgroup of positively correlated parameters consisting of C^α-E_σ^{L→M} (EDA), Σσ_m and Σσ_p (Hammett), C⁴⁵-δ(¹³C) and H⁴⁵-δ(¹H) (NMR, experimental) was found to be negatively correlated to C²-E_σ^{L←M} (EDA) (Fig. 6b, group 2).

3. Another subgroup of positively correlated parameters consisting of C²-E_π (EDA), C²-δ(¹³C) NMR (experimental and



a) Group 1 = EDA: C^α-E_π^{L→M} (13), EDA: C²-E_π^{L←M} (29), NMR (DFT): C²-δ(¹³C) (49) and pK_a (58)

b) Group 2 = EDA: C^α-E_σ^{L→M} (11), EDA: C²-E_σ^{L←M} (27), Hammett: Σσ_m (34), Hammett: Σσ_p (36), NMR: C⁴⁵-δ(¹³C) (46) and NMR: H⁴⁵-δ(¹H) (52)



c) Group 3 (modelled) = EDA: C²-E_π (24), NMR: C²-δ(¹³C) (49), structure: d(Au-C²) (86) and structure: d(Au-C^α) (88)

d) Group 4 (modelled) = NMR: C²-δ(¹³C) (49), order: B(C^α-Au) (55), order: B(C^α-H^α) (57), structure: ∠N¹-C²-N³ (78), structure: σ(C^α-Au) (84) and structure: d(Au-C²) (86)

Fig. 6 Correlation graphs of selected parameters. Vertices are numbered and edges are coloured by set: EDA (plum), NMR (red), pK_a (grey), Hammett (orange), structure (brown) and order (wood).⁶¹ Blue and red vertices represent positive and negative Spearman correlations⁶² between vertices, respectively. Vertices with lower weights indicate correlations with higher false-discovery rate adjusted *p*-values.⁶³

modelled) and *d*(Au-C²) (structure) was found to be negatively correlated with structural parameter *d*(Au-C^α) (Fig. 6c, group 3).

4. Negative correlations were found between ∠N¹-C²-N³ (structure) and *B*(C^α-Au) (order) and *d*(Au-C²) (structure), whereas the latter two parameters were found mutually positively correlated (Fig. 6d, group 4). Correlations between these parameters and related parameters *B*(C^α-H^α) (order) was lower and except for *B*(C^α-H^α), all parameters were highly correlated with NMR (DFT): C²-δ(¹³C).

Point-to-point regression models

Selected one-variable linear relations revealed trends in the data of [Au(IPr)(CHR₂)] 3–12 (Table 4).⁶⁶ Specific parameters from the EDA related to modelled NMR chemical shifts and pK_a values (Table 4, entries 1–4, group 1).⁶⁷ Properties obtained from the EDA, C^α-E_π^{L→M} and C²-E_π^{L←M}, were found to be inversely proportional and proportional, respectively, to both C²-δ(¹³C) (NMR, modelled) and pK_a. These latter two parameters were found to be proportional as well (*R*² = 0.71, *p*-value < 0.01), and a statistically significant inverse relation was found between C^α-E_π^{L→M} and C²-E_π^{L←M} (EDA, *R*² = 0.92,

Table 4 Selected linear relations (part A)^a

Entry	Equation	R ²
Group 1: EDA, NMR and pK_a		
1 ^b	EDA: C ^α -E _π ^{L→M} ∝ -C ² -δ(13C)	0.93
2 ^b	EDA: C ² -E _π ^{L→M} ∝ C ² -δ(13C)	0.96
3	EDA: C ^α -E _π ^{L→M} ∝ -pK _a	0.94
4	EDA: C ² -E _π ^{L→M} ∝ pK _a	0.91
Group 2: EDA and NMR versus Hammett		
5	EDA: C ^α -E _σ ^{L→M} ∝ ∑σ _m	0.96
6	EDA: C ² -E _σ ^{L→M} ∝ ∑σ _m	0.91
7 ^c	NMR: C ⁴⁵ -δ(13C) ∝ ∑σ _p	0.92
8 ^c	NMR: H ⁴⁵ -δ(1H) ∝ ∑σ _p	0.95
Group 3: EDA and structure versus NMR^d		
9 ^b	EDA: C ² -E _π ∝ C ² -δ(13C)	0.92
10 ^b	Struct.: d(Au-C ²) ∝ C ² -δ(13C)	0.96
11 ^b	Struct.: d(Au-C ^α) ∝ -C ² -δ(13C)	0.88
Group 4: Order versus NMR and structure		
12 ^b	B(C ^α -Au) ∝ C ² -δ(13C)	0.95
13 ^b	B(C ^α -Au) ∝ σ(C ^α -Au)	0.78
14 ^b	B(C ^α -H ^α) ∝ -∠N ¹ -C ² -N ³	0.93
15 ^b	B(C ^α -H ^α) ∝ d(Au-C ²)	0.97

^a Corresponding regression plots are presented in the ESI. Struct. = structure. ^b Modelled values (DFT) used. ^c Experimental values used. ^d Analogous models with experimental values gave lower R² values of 0.89, 0.46 and 0.70.

p-value = 0.01). From these relations, it followed that the dominant donation of electron density from C^α to gold (Table 3) was increased with more Brønsted basic carbanions (CHR₂⁻, with higher pK_a of corresponding CH₂R₂ protons), while the minor (Table 3) donation of electron density from gold to C² was reduced.

Other parameters from the EDA and different experimental NMR chemical shifts related to different derived Hammett parameters (Table 4, entries 5–8, group 2). The positive correlations between C^α-E_σ^{L→M}, C²-E_σ^{L→M} (EDA) and ∑σ_m (Hammett) and those between C⁴⁵-δ(13C), H⁴⁵-δ(1H) (NMR) and ∑σ_p (Hammett) were found to be statistically significant. Note that the statistically significant relation between C^α-E_σ^{L→M} and C²-E_σ^{L→M} was excellent as well (R² = 0.99, *p*-value < 0.01). The inverse relation between pK_a and either ∑σ_m (R² = 0.73, *p*-value = 0.01) and ∑σ_p (R² = 0.64, *p*-value = 0.02) warranted an analogous analysis as in the prior group of parameters. Thus, carbanions (CHR₂⁻) bearing more strongly electron donating substituents appeared to engage in a bonding interaction with stronger σ-donation through gold and stronger σ-backbonding (of approximately equal magnitude, Table 3) to the NHC ligand. The effect coincided with shielded C⁴⁵-δ(13C) and H⁴⁵-δ(1H) chemical shift values, indicative of larger electron density in the π-system of the NHC.

Further relations based on C²-δ(13C) chemical shift values were found (Table 4, entries 9–10, group 3). Next to the previously discussed relation of modelled chemical shift C²-δ(13C) with directed π-bonding interactions (bonding from C^α, back-bonding to C², Table 4, entries 1 and 2), chemical shifts C²-δ(13C) were found to relate with the EDA parameter associated with the combined π-bonding energy in the C²-Au bond, C²-E_π

(Table 4, entry 9). The chemical shift C²-δ(13C) also related to bond distances d(Au-C²) and d(Au-C^α) (Table 4, entries 10 and 11): higher values of C²-δ(13C) (as an indication of lower electron density on the gold centre) would result from more strongly donating carbanion ligands (CHR₂⁻) that would have stronger (shorter) Au-C^α bonds and weaker (longer) Au-C² bonds to effectively transfer the electron density.⁴⁶

Relations were found between Wiberg bond order values and parameters associated with NMR chemical shifts and structural parameters (Table 4, entries 12–15, group 4). NMR parameter C²-δ(13C) was found to relate with B(C^α-Au) (Table 4, entry 12), in agreement with variations in bond length d(Au-C^α) (Table 4, entry 11). The relation of B(C^α-Au) to Coulson parameter σ(C^α-Au) (Table 4, entry 13), suggested that differences in modelled bond orders might be influenced by the proportion of different atomic orbitals (s and p) in the molecular orbitals; a balance between interaction of σ and π symmetry would clearly be influenced by the s character of bonding orbitals. Support for this hypothesis was found in an inverse linear relation between structural parameters ∠N¹-C²-N³ and σ(C^α-Au) (R² = 0.75, *p*-value < 0.01). Here, a higher s character in the orbital of C^α bound to gold appeared to coincide with a higher s character of the σ-type orbital on C².³⁴ Wiberg bond orders for the bonds between C^α and H^α, B(C^α-H^α), were found to be inversely proportional to ∠N¹-C²-N³ and proportional to d(Au-C²) (Table 4, entries 14 and 15) suggested that the particular bonding arrangement in the carbanion ligand (CHR₂⁻) coincided with changes in the bond length to gold and manifested itself in the carbene angle of the NHC ligand. Absence of a statistically significant relation between B(C^α-H^α) and B(C^α-Au) prohibited meaningful *inter alia* comparison of all Wiberg bond order values.

Point-to-plane regression models

Various point-to-plane relations with planes defined by multiple parameters were found to capture additional trends (Table 5). When structural parameters d(C⁴⁵-N¹³) and previously encountered Coulson parameter σ(C^α-Au) (Table 4, entry 13) were combined, they were found to relate to the modelled %s-character of C^α in fragments CHR₂⁻, C^α_s ≥ 0.5 (Table 5, entry 1). This relation hinted that C^α_s ≥ 0.5 might be used to predict structural effect in complexes [Au(IPr)(CHR₂)],

Table 5 Selected linear relations (part B)^a

Entry	Equation	R ²
Group 5: Two-parameter models (structure)		
1 ^b	Component: C ^α _s ≥ 0.5 ∝ σ(C ^α -Au) - d(C ⁴⁵ -N ¹³)	0.91
2 ^b	Order: B(C ^α -Au) ∝ σ(C ^α -Au) + d(C ⁴⁵ -N ¹³)	0.90
3 ^b	NMR: C ² -δ(13C) ∝ σ(C ^α -Au) + d(C ⁴⁵ -N ¹³)	0.89
Group 6: Multi-parameter models (NMR)		
4 ^b	pK _a ∝ C ² -δ(13C)-C ^α -δ(13C)-C ⁴⁵ -δ(13C)	0.98
5 ^c	log <i>k</i> _{rel} ∝ C ^α -δ(13C)-C ² -δ(13C)-H ^α -δ(1H)-H ⁴⁵ -δ(1H)	0.87

^a Corresponding regression plots are presented in the ESI. ^b Modelled values (DFT) used. ^c Experimental values used.

however, the respective explaining values (85% and 6%)⁶⁸ and suggests that $d(C^{4/5}-N^{1/3})$ should be omitted. $B(C^\alpha-Au)$ could be related to either structural parameter $\angle N^1-C^2-N^3$ or $d(Au-C^2)$ (Table 4, entries 15 and 16), but a combination of two different parameters, $\sigma(C^\alpha-Au)$ and $d(C^{4/5}-N^{1/3})$ was found to give an alternative description (Table 5, entry 2). The latter parameter remained (as in Table 5, entry 1) of low explaining power (21%), while the former one explained the majority (69%) of the variation in $B(C^\alpha-Au)$. Modelled NMR chemical shift $C^2-\delta(^{13}C)$ could be related to a combination of the same two structural parameters (Table 5, entry 3), with explaining powers of 52% and 37%, respectively. The analogous model for experimental parameters provided an even better fit ($R^2 = 0.94$, p -value < 0.01).⁶⁹

Planes defined by the regression coefficients of linear models based on $\sigma(C^\alpha-Au)$ and $d(C^{4/5}-N^{1/3})$ (Table 5, entries 1–3), gave insight in the structure of the underlying data (Fig. 7). The opposite sign for structural parameter $d(C^{4/5}-N^{1/3})$ in the model for $C^\alpha_s \geq 0.5$ (component) relative to that in the models for $B(C^\alpha-Au)$ (order) and $C^2-\delta(^{13}C)$ (NMR) is visually apparent from an intersection of the two planes. The tilt between the planes defined by the models for two-parameter models for $B(C^\alpha-Au)$ (order) and $C^2-\delta(^{13}C)$ (NMR) highlighted the difference in values of the coefficients with matching signs while the linear relation between those dependent variables remained excellent ($R^2 = 0.95$, p -value < 0.01).

With the wide range of relations between NMR chemical shifts and other parameters established, models with three or four such parameters were evaluated (Table 5, entries 4 and 5, group 6). A three-variable model for pK_a with a positive sign for $C^2-\delta(^{13}C)$ and negative signs for $C^\alpha-\delta(^{13}C)$ and $C^{45}-\delta(^{13}C)$ were found when modelled NMR chemical shifts were used (Table 5, entry 4). The different parameters contributed in a balanced manner, with values of 31%, 27% and 40%, respectively. A four-variable model (Table 5, entry

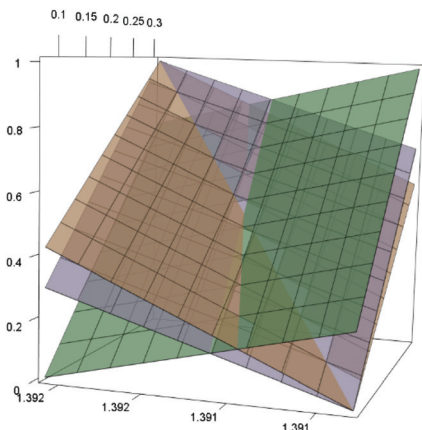


Fig. 7 Surface plots of selected regression models. Planes (Table 5, entries 6–8) are scaled and translated along their intercepts to span values between 0 and 1 for the range of values for $d(C^{4/5}-N^{1/3})$ and $\sigma(C^\alpha-Au)$. (A) Component: $C^\alpha_s \geq 0.5$ (green); (B) order: $B(C^\alpha-Au)$ (purple); and (C) NMR: $C^2-\delta(^{13}C)$ (modelled, orange).⁷⁰

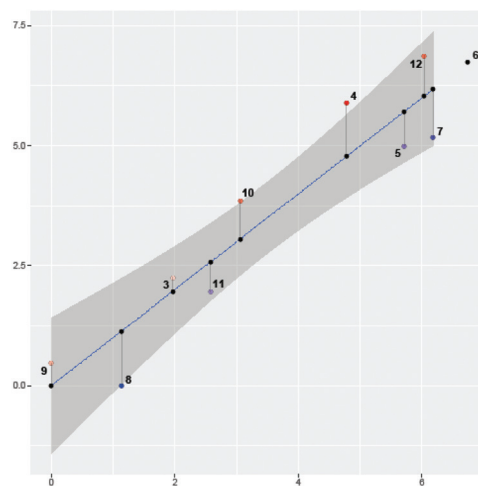


Fig. 8 Regression model of $\log k_{rel}$ versus NMR parameters. $\log k_{rel} = 998 + 0.212 \times C^\alpha-\delta(^{13}C) - 1.596 \times C^2-\delta(^{13}C) - 566 \times H^\alpha-\delta(^1H) - 95.69 \times H^{45}-\delta(^1H)$ (Table 5, entry 11). Measured and fitted $\log k_{rel}$ values are plotted as coloured and black points, respectively. Numbers refer to complexes 3–12. Colours (red and blue) and shades indicate relative position and distance from fitted values. The shaded area represents the confidence interval of the linear model (at 95%).

5) based on experimental NMR chemical shifts was found suitable for the description of the relative tendencies of protodeauration of $[Au(IPr)(CHR_2)]$ (3–5 and 7–12) (Fig. 3). This model included coefficients with a positive sign for $C^\alpha-\delta(^{13}C)$ and negative signs for chemical shifts $C^2-\delta(^{13}C)$, $H^\alpha-\delta(^1H)$ and $H^{45}-\delta(^1H)$, with relative contribution values of 40%, 11%, 21% and 14%, respectively (Fig. 8). Importantly, even though no relation was found between $\log k_{rel}$ and pK_a ($R^2 = 0.05$), the mutual signs of $C^2-\delta(^{13}C)$ and $C^\alpha-\delta(^{13}C)$ persisted. Consistency of the signs of the coefficient for derived Hammett parameter $\sum \sigma_p$ in models for experimental $C^{45}-\delta(^{13}C)$ and $H^{45}-\delta(^1H)$ chemical shifts (Table 4, entries 7 and 8) was as expected from their mutual relation ($R^2 = 0.85$, p -value < 0.01) as well.

The presence of parameters with symmetry labels σ and π in the different groups (Tables 4 and 5) was used to designate parameters to the two groups. The pK_a values of CH_2R_2 and chemical shift $C^2-\delta(^{13}C)$ parameters (group 1) and structural parameters $d(Au-C^\alpha)$ and $\angle N^1-C^5-C^4-N^3$ (group 3) could be associated with π symmetry. NMR parameters $C^{45}-\delta(^{13}C)$ and $H^{45}-\delta(^1H)$ (group 2), structural parameters $d(Au-C^2)$ and $d(Au-C^2)$ and parameters describing bond orders (group 4) could be associated with σ symmetry. The relations found added quantitative support the spectroscopically suggested trend of transfer of electron density from carbanion ligands (CHR_2^-) to the $[Au(IPr)]^+$ fragments (Table 1). No strong support was found for the structurally suggested trends of bent $\angle C^2-Au-C^\alpha$ bonds and twisted imidazole cores in the IPr ligand (Table 2), but relations between other structural parameters such as $d(C^{4/5}-N^{1/3})$, $\sigma(C^\alpha-Au)$ and different bond orders provided insight into the hybridisation and distribution of electron density in different parts of $[Au(IPr)(CHR_2)]$.

Summary of linear relations

The presence of parameters with symmetry labels σ and π in the different groups (Tables 4 and 5) was used to designate parameters to the two groups. The pK_a values of CHR_2 and chemical shift $\text{C}^{2-}\delta(^{13}\text{C})$ parameters (group 1) and structural parameters $d(\text{Au}-\text{C}^\alpha)$ and $\angle\text{N}^1-\text{C}^5-\text{C}^4-\text{N}^3$ (group 3) could be associated with π symmetry. NMR parameters $\text{C}^{45-}\delta(^{13}\text{C})$ and $\text{H}^{45-}\delta(^1\text{H})$ (group 2), structural parameters $d(\text{Au}-\text{C}^2)$ and $d(\text{Au}-\text{C}^2)$ and parameters describing bond orders (group 4) could be associated with σ symmetry. The relations found added quantitative support the spectroscopically suggested trend of transfer of electron density from carbanion ligands (CHR_2^-) to the $[\text{Au}(\text{IPr})]^+$ fragments (Table 1). No strong support was found for the structurally suggested trends of bent $\angle\text{C}^2-\text{Au}-\text{C}^\alpha$ bonds and twisted imidazole cores in the IPr ligand (Table 2), but relations between other structural parameters such as $d(\text{C}^{4/5}-\text{N}^{1/3})$, $\sigma(\text{C}^\alpha-\text{Au})$ and different bond orders provided insight into the hybridisation and distribution of electron density in different parts of $[\text{Au}(\text{IPr})(\text{CHR}_2)]$ (Fig. 5).

Conclusions

The range of NHC–gold(i) complexes with sp^3 -hybridised carbanion auxiliary ligands has been expanded and their relative rates of protodeauration have been measured. A wealth of spectroscopic and structural data was collected, and computational models were generated to quantify various electronic properties. Substitution of the carbanion ligand (CHR_2^-) was found to have a profound effect on both steric and electronic properties, not only in this ligand itself, but in the bonds to gold and the NHC ligand as well. Computational EDA studies separated electronic interactions in σ/π and bonding/back-bonding constituents. A combination of path analysis and correlation analysis was used to unravel relations between different parameters and a number of trends were corroborated with statistically significant regression models. Theoretical parameters such as pK_a and Hammett constants could be used to relate these effects and NMR chemical shifts of various parts of the complexes were found indicative as well. Variations in structural parameters exemplified the ability of the ligands to adjust to varying electronic configuration. This study has shown that quantitative models of varying complexity can indeed effectively be distilled from a diverse set of chemical data without *a priori* knowledge about the mutual relations between different parameters. Application of this approach to related chemical systems and development of the methods to a general analytical framework will be subject of future contributions.

Abbreviations

DCD Dewar–Chatt–Duncanson;
DFT Density functional theory

EDA Energy decomposition analysis
FDR False discovery rate
IR Infrared
IPr 1,3-Bis(2,6-diisopropylphenyl)imidazol-2-ylidene
tBu 1,3-Bis(tertbutyl)imidazol-2-ylidene
NHC N-Heterocyclic carbene
NMR Nuclear magnetic resonance.

Crystallography data

CCDC 1811379 (for 7), 1811380 (for 8), 1811381 (for 9), 1811382 (for 10), 1811383 (for 11) and 1811384 (for 12) contain the supplementary crystallographic data for this paper.

Conflicts of interest

Authors declare no competing financial interests.

Acknowledgements

The European Research Council (ERC) and the Engineering and Physical Sciences Research Council (EPSRC), UK, are gratefully acknowledged for their support. Umicore AG is thanked for generous donations of auric acid. L. C., and S. P. N. thank the King Abdullah University of Science and Technology (KAUST) and King Saud University (KSU) for support. We also thank the KAUST Supercomputing Laboratory housing the Shaheen II supercomputer for providing the computational resources. Dr Liam Ball is thanked for his help with the kinetics data analysis. L. M. A. is an ULPGC Postdoc Fellow, and thanks Universidad de Las Palmas de Gran Canaria (ULPGC).

Notes and references

- (a) I. Braun, A. M. Asiri and A. S. K. Hashmi, *ACS Catal.*, 2013, **3**, 1902; (b) C. Obradors and A. M. Echavarren, *Acc. Chem. Res.*, 2014, **47**, 902.
- A. S. K. Hashmi, *Gold Bull.*, 2003, **36**, 3.
- (a) S. Gaillard, C. S. J. Cazin and S. P. Nolan, *Acc. Chem. Res.*, 2011, **45**, 778; (b) G. Zhang, Y. Luo, Y. Wang and L. Zhang, *Angew. Chem., Int. Ed.*, 2011, **50**, 4450.
- (a) P. H.-Y. Cheong, P. Morganelli, M. R. Luzung, K. N. Houk and F. D. Toste, *J. Am. Chem. Soc.*, 2008, **130**, 4517; (b) A. S. K. Hashmi, T. D. Ramamurthi and F. Rominger, *J. Organomet. Chem.*, 2009, **694**, 592; (c) A. S. K. Hashmi, *Angew. Chem., Int. Ed.*, 2010, **49**, 5232; (d) W. Wang, G. B. Hammond and B. Xu, *J. Am. Chem. Soc.*, 2012, **134**, 5697; (e) B. Ranieri, I. Escofet and A. M. Echavarren, *Org. Biomol. Chem.*, 2015, **13**, 7103; (f) F. Rekhroukh, L. Estevez, S. Mallet-Ladeira, K. Miqueu,

- A. Amgoune and D. Bourissou, *J. Am. Chem. Soc.*, 2016, **11920**–11929.
- 5 P. Pyykkö, *Angew. Chem., Int. Ed.*, 2004, **43**, 4412.
- 6 S. Patai and Z. Rappoport, *The Chemistry of Organic Derivatives of Gold and Silver*, Wiley, 1999.
- 7 G. C. Fortman, A. Poater, J. W. Levell, S. Gaillard, A. M. Z. Slawin, I. D. W. Samuel, L. Cavallo and S. P. Nolan, *Dalton Trans.*, 2010, **39**, 10382.
- 8 (a) G. Xu, C. Zhu, W. Gu, J. Li and J. Sun, *Angew. Chem., Int. Ed.*, 2014, **54**, 883; (b) T. C. Boorman and I. Larrosa, *Chem. Soc. Rev.*, 2011, **40**, 1910; (c) M. R. Fructos, M. M. Díaz-Requejo and P. J. Pérez, *Chem. Commun.*, 2016, **52**, 7326; (d) S. Kramer, *Chem. – Eur. J.*, 2016, 15584; (e) Z. Zheng, Z. Wang, Y. Wang and L. Zhang, *Chem. Soc. Rev.*, 2016, **45**, 4448.
- 9 (a) S. Bhunia, S. Ghorpade, D. B. Huple and R.-S. Liu, *Angew. Chem., Int. Ed.*, 2012, **51**, 2939; (b) J. Xie, C. Pan, A. Abdukader and C. Zhu, *Chem. Soc. Rev.*, 2014, **43**, 5245; (c) G. Zhang, Y. Luo, Y. Wang and L. Zhang, *Angew. Chem., Int. Ed.*, 2011, **50**, 4450.
- 10 M. B. Smith and J. March, *March's Advanced Organic Chemistry: Reactions, Mechanisms, and Structure*, Wiley-Interscience, 2007, pp. 381–382.
- 11 H. Schmidbauer, *Gold: Chemistry, Biochemistry and Technology*, Wiley, 1999.
- 12 S. Bhunia, S. Ghorpade, D. B. Huple and R.-S. Liu, *Angew. Chem., Int. Ed.*, 2012, **51**, 2939.
- 13 (a) Y. Zhu, C. S. Day and A. C. Jones, *Organometallics*, 2012, **31**, 7332; (b) M. Sriram, Y. Zhu, A. M. Camp, C. S. Day and A. C. Jones, *Organometallics*, 2014, **33**, 4157.
- 14 S. Ma, S. Yu and Z. Gu, *Angew. Chem., Int. Ed.*, 2006, **45**, 200.
- 15 IPr = 1,3-bis(2,6-diisopropylphenyl)imidazol-2-ylidene.
- 16 F. G. Bordwell, *Acc. Chem. Res.*, 1988, **21**, 456.
- 17 W. N. Olmstead, Z. Margolin and F. G. Bordwell, *J. Org. Chem.*, 1980, **45**, 3295.
- 18 E. M. Arnett, S. G. Maroldo, S. L. Schilling and J. A. Harrelson, *J. Am. Chem. Soc.*, 1984, **106**, 6759.
- 19 W. S. Matthews, J. E. Bares, J. E. Bartmess, F. G. Bordwell, F. J. Cornforth, G. E. Drucker, Z. Margolin, R. J. McCallum, G. J. McCollum and N. R. Vanier, *J. Am. Chem. Soc.*, 1975, **97**, 7006.
- 20 F. G. Bordwell, J. E. Bares, J. E. Bartmess, G. J. McCollum, M. van der Puy, N. R. Vanier and W. S. Matthews, *J. Org. Chem.*, 1977, **42**, 321.
- 21 R. P. Bell and W. C. E. Higginson, *Proc. R. Soc. A*, 1949, **197**, 141.
- 22 P. de Frémont, N. M. Scott, E. D. Stevens and S. P. Nolan, *Organometallics*, 2005, **24**, 2411.
- 23 S. Gaillard, A. M. Z. Slawin and S. P. Nolan, *Chem. Commun.*, 2010, **46**, 2742.
- 24 (a) W. A. Herrmann, *Angew. Chem., Int. Ed.*, 2002, **41**, 1290; (b) N. Marion and S. P. Nolan, *Chem. Soc. Rev.*, 2008, **37**, 1776; (c) D. J. Gorin, B. D. Sherry and F. D. Toste, *Chem. Rev.*, 2008, **108**, 3351; (d) S. P. Nolan, *Acc. Chem. Res.*, 2011, **44**, 91.
- 25 V. J. Scott, J. A. Labinger and J. E. Bercaw, *Organometallics*, 2010, **29**, 4090.
- 26 D. Gasperini, A. Collado, A. Gómez-Suárez, D. B. Cordes, A. M. Z. Slawin and S. P. Nolan, *Chem. – Eur. J.*, 2015, **21**, 5403.
- 27 I. I. F. Boogaerts and S. P. Nolan, *J. Am. Chem. Soc.*, 2010, **132**, 8858.
- 28 D. Emeljanenko, A. Peters, V. Vitske, E. Kaifer and H.-J. Himmel, *Eur. J. Inorg. Chem.*, 2010, 4783.
- 29 A. Pross, D. J. DeFrees, B. A. Levi, S. K. Pollack, L. Radom and W. J. Hehre, *J. Org. Chem.*, 1981, **46**, 1693.
- 30 C. Hansch, A. Leo and R. W. Taft, *Chem. Rev.*, 1991, **91**, 165.
- 31 R. Credendino, L. Falivene and L. Cavallo, *J. Am. Chem. Soc.*, 2012, **134**, 8127.
- 32 O. Back, M. Henry-Ellinger, C. D. Martin, D. Martin and G. Bertrand, *Angew. Chem., Int. Ed.*, 2013, **52**, 2939.
- 33 (a) S. V. C. Vummaleti, D. J. Nelson, A. Poater, A. Gómez-Suárez, D. B. Cordes, A. M. Z. Slawin, S. P. Nolan and L. Cavallo, *Chem. Sci.*, 2015, **6**, 1895; (b) D. Marchione, M. A. Izquierdo, G. Bistoni, R. W. A. Havenith, A. Macchioni, D. Zuccaccia, F. Tarantelli and L. Belpassi, *Chem. – Eur. J.*, 2017, 2722.
- 34 A. Comas-Vives and J. N. Harvey, *Eur. J. Inorg. Chem.*, 2011, **2011**, 5025.
- 35 I. V. Alabugin, S. Bresch and G. dos Passos Gomes, *J. Phys. Org. Chem.*, 2015, **28**, 147.
- 36 (a) M. A. Oquendo, E. Baca-Garcia, A. Artés-Rodríguez, F. Perez-Cruz, H. C. Galfalvy, H. Blasco-Fontecilla, D. Madigan and N. Duan, *Mol. Psychiatry*, 2012, **17**, 956; (b) T. J. Carney, G. P. Morgan, J. Jones, A. M. McDaniel, M. T. Weaver, B. Weiner and D. A. Haggstrom, *J. Biomed. Inf.*, 2015, **57**, 288.
- 37 Even though most reactions proceeded at rt, the reaction mixtures were heated to 60 °C or 80 °C to ensure rapid and complete conversion. Due to the low tendency of gold(i) complexes to undergo β -hydride elimination, **12** is unlikely to decompose *via* such a pathway.^{4f}
- 38 The high pK_a of **2** suggests that it might be able to deprotonate chloroform. Experimental investigations to the formation of dichlorocarbene complexes will be subject of future investigations.
- 39 J. Vicente, M.-T. Chicote and M.-C. Lagunas, *Helv. Chim. Acta*, 1999, **82**, 1202.
- 40 J. F. Box, *Stat. Sci.*, 1987, **2**, 45–52.
- 41 K. E. Roth and S. A. Blum, *Organometallics*, 2010, **29**, 1712.
- 42 Description of the experimental procedure and transformation of the data are given in the ESI.†
- 43 E. Limpert, W. A. Stahel and M. Abbt, *Bioscience*, 2001, **51**, 341.
- 44 R. M. Beesley, C. K. Ingold and J. F. Thorpe, *J. Chem. Soc., Dalton Trans.*, 1915, **107**, 1080.
- 45 G. A. Olah, *Acc. Chem. Res.*, 1971, **4**, 240.
- 46 M. V. Baker, P. J. Barnard, S. K. Brayshaw, J. L. Hickey, B. W. Skelton and A. H. White, *Dalton Trans.*, 2005, 37.
- 47 L. P. Wolters and F. M. Bickelhaupt, *ChemistryOpen*, 2013, **2**, 106.

- 48 Relevant values and discussion is given in the ESI.†
- 49 D. M. Root, C. R. Landis and T. Cleveland, *J. Am. Chem. Soc.*, 1993, **115**, 4201.
- 50 In a tetrahedral arrangement of C^α , an average of the bonds angles $Au-C^\alpha-X$ ($X = H, R^1, R^2$) approaching 109.5° would be expected. The Droop angle is defined as the average angle between a plane defined by H, R^1 and R^2 , positioned at C^α , and each of H, R^1 and R^2 . Values for θ thus range between 0° (flat) and 19.5° (tetrahedral).
- 51 F. Weinhold and C. R. Landis, *Valency and Bonding: A Natural Bond Orbital Donor-Acceptor Perspective*, Cambridge University Press, 2005.
- 52 Formulae and values are given in the ESI.†
- 53 In a fully symmetrical tetrahedral arrangement, the orbital that engages in a bonding interaction with gold would be a sp^3 hybridised orbital with 25% s-character.
- 54 S. Gaillard, A. M. Z. Slawin, A. T. Bonura, E. D. Stevens and S. P. Nolan, *Organometallics*, 2010, **29**, 394.
- 55 (a) J. S. Dewar, *Bull. Soc. Chim. Fr.*, 1951, **18**, C71–C79; (b) J. Chatt and L. A. Duncanson, *J. Chem. Soc.*, 1953, 2939.
- 56 (a) C. Boehme and G. Frenking, *Organometallics*, 1998, **17**, 5801; (b) B. Venkataraman, *J. Chem. Educ.*, 2017, 296; (c) D. Benitez, N. D. Shapiro, E. Tkatchouk, Y. Wang, W. A. Goddard III and F. D. Toste, *Nat. Chem.*, 2009, **1**, 482.
- 57 (a) D. Nemcsok, K. Wichmann and G. Frenking, *Organometallics*, 2004, **23**, 3640; (b) H. Jacobsen, A. Correa, C. Costabile and L. Cavallo, *J. Organomet. Chem.*, 2006, **691**, 4350; (c) R. Tonner, G. Heydenrych and G. Frenking, *Chem. – Asian J.*, 2007, **2**, 1555.
- 58 All values are given in the ESI.†
- 59 A. J. Bridgeman, G. Cavigliasso, L. R. Ireland and J. Rothery, *J. Chem. Soc., Dalton Trans.*, 2001, 2095.
- 60 S. Saha, R. K. Roy and P. W. Ayers, *Int. J. Quantum Chem.*, 2009, **109**, 1790.
- 61 Parameters are numbered for clarity, a full numbering scheme of parameters from all sets is given in the ESI.†
- 62 C. Spearman, *Am. J. Psychol.*, 1904, **15**, 72.
- 63 Y. Benjamini and Y. Hochberg, *J. R. Stat. Soc., B*, 1995, **57**, 289.
- 64 Analysis of all data is detailed in the ESI.†
- 65 Information in parentheses indicates the group of the parameters and/or whether the data is derived from experimental measurements or from the modelling studies.
- 66 Additional correlations and linear models are given in sections 11 and 12 of the ESI.†
- 67 Choice for use of experimental or modelled values is based on both the quality of the linear models.
- 68 U. Grömping, *J. Stat. Softw.*, 2006, **17**, 1.
- 69 With explaining powers of 48% and 46% for the two explanatory variables.
- 70 All coefficients and scaled values are given in the ESI.†